

A Friction-Based Finite Element Analysis of Ultrasonic Consolidation

In this study, the contribution of friction to the bonding mechanism in ultrasonic welding is explored, and offered are the distributions of temperature and plastic deformation caused by the friction stress

BY C. ZHANG AND L. LI

ABSTRACT. Surface bond formation in ultrasonic consolidation is a complicated thermal-mechanical coupled process. Friction and plastic flow are used to simulate the bond interface behavior. This paper focuses on the contribution of friction to the bonding mechanism in ultrasonic welding. Based on a 3-D thermomechanical quasi-static finite element model, the distributions of temperature and plastic deformation caused by the friction stress are presented. Temperature and plastic deformation are found to vary with vibration cycles. A saturation phenomenon is identified that after a certain number of vibration cycles, the plastic deformation at the bond interface reaches a steady state.

Introduction

The ultrasonic consolidation (UC) process is designed to continuously weld layers of metal foil to previously deposited layers, during which the profile to each layer is created by contour milling, to build up a 3-D structure. As with ultrasonic welding, most commercially available metal foils, such as aluminum, titanium, magnesium, copper, and steel, can be used in the UC process (Refs. 1, 2).

One area that will benefit from an improved understanding of ultrasonic bonding is the fabrication of metal matrix composites (MMCs). Continuous fiber-reinforced MMCs are typically produced using diffusion bonding or casting, whereas discontinuously reinforced MMCs are typically produced using powder metallurgy or pressure-assisted casting methodologies (Ref. 3). The appropriate design and application of MMCs depends on how easily they can be fabricated. The ability to model their properties accurately is one of the keys to the ef-

fective implementation of MMCs in new and existing applications.

As a joining method, ultrasound bonding is arguably the least understood. However, realization of the full potential of ultrasonic bonding will require a greater understanding of the mechanisms for bond formation. No systematic simulation results and analysis have been published on ultrasonic bonding, especially those of the interface between the top layer of the foil and the substrate that is believed to be the most important region where bonding occurs. Most research of UC assumes that friction and plastic flow can be studied to understand the most fundamental phenomena at the interface in ultrasonic welding (Refs. 2, 4–9). The friction is attributed as the shear effect on bonding, while plastic deformation is attributed as the process in which the bond forms. Diffusion is also suggested as a possible process for bond formation; however, the relatively low temperature and short time during the rapid bonding process seem to make diffusion insignificant for bond formation.

Coupled Physical Phenomena in Ultrasonic Consolidation

The bond formation between the foil and substrate in UC is still unknown to researchers because of the complicated interactions of vibration, deformation, friction-like shear, localized thermal effect, and oxides/contaminants dispersion on the interface. The modeling of ultrasonic

consolidation of metals and alloys began only recently with the development of emerging new technologies that employ ultrasonic welding in ultrasonic consolidation. The weld strength of UC was modeled and an empirical model was derived on the basis of the theory of surface and volume effects by Kong et al. (Ref. 10). A 2-D spot-welding model for the mechanical field was also constructed, and the variation of friction coefficient during the process was measured and studied in detail by Gao and Doumanidis (Ref. 11). Their results pointed out the role of friction and pressure in the formation of the elastic strain field at the bond region. However, since the heat equation was not included in their analysis, the results did not include any thermal effect.

This paper attempts to present the effect of friction on the bonding interface by applying Coulomb's law of friction, and assumes that, under the vibration load, the interface material will go through the localized elastoplastic deformation under the friction heating process.

During ultrasonic consolidation, the behavior of the bonding interface can be described as follows: 1) The sonotrode vibrates at a fixed frequency transversely to the direction of sonotrode travel (Fig. 1) and a constant pressure is applied through the sonotrode; 2) the friction at the contact surface area will break the surface contaminants, such as oxides, so as to build an intimate contact condition; 3) the ultrasonic vibration generates a localized elevated-temperature zone at the contact surface, which will dramatically reduce the critical shear stress; and 4) shear strain in turn will generate heat and affect the friction conditions. Therefore, the ultrasonic consolidation is a continuous process in which the generation of strain in the mechanical field and temperature in the thermal field are interactive. Thus, the UC process constitutes a typical coupled-field problem.

The analysis strategy for ultrasonic consolidation as a coupled-field problem is outlined in Fig. 2. It can be seen that in the

KEYWORDS

Numerical Model
Ultrasonic Consolidation (UC)
Friction
Thermal-Mechanical Analysis
Plastic Strain
Bond Formation

C. ZHANG is a PhD student and L. LI (leijun.li@usu.edu) is a faculty member with the Department of Mechanical & Aerospace Engineering at Utah State University, Logan, Utah.

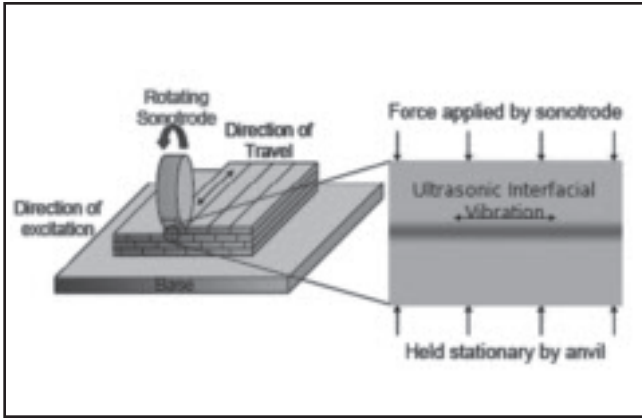


Fig. 1 — Schematic of ultrasonic consolidation process based on Ref. 12.

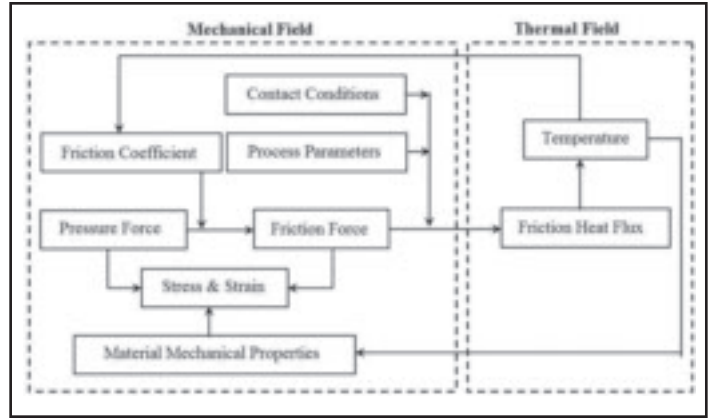


Fig. 2 — Diagram showing the process parameters, mechanical properties, and possible interactions (couplings) between thermal and mechanical mechanisms for ultrasonic consolidation (Ref. 13).

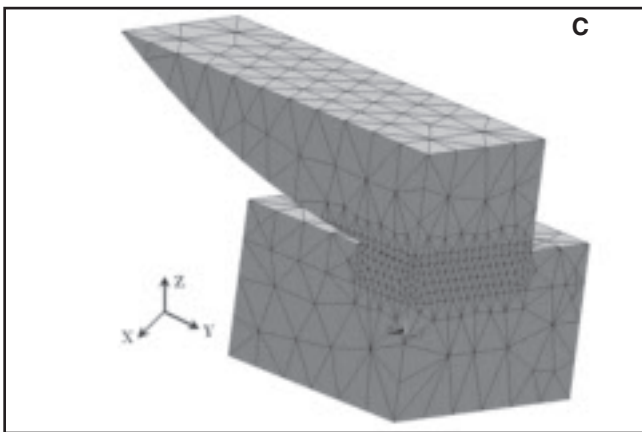
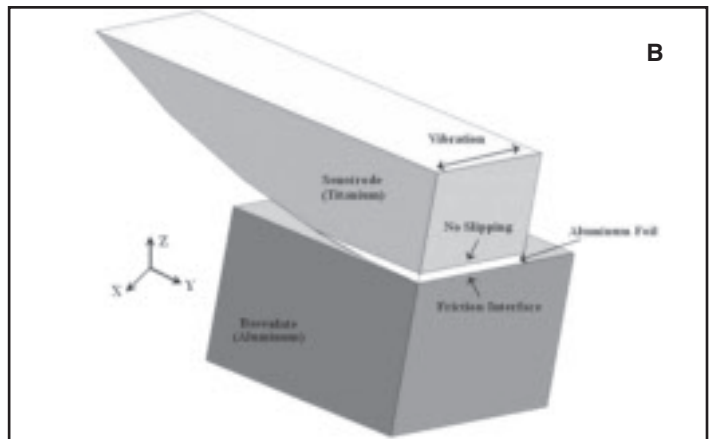
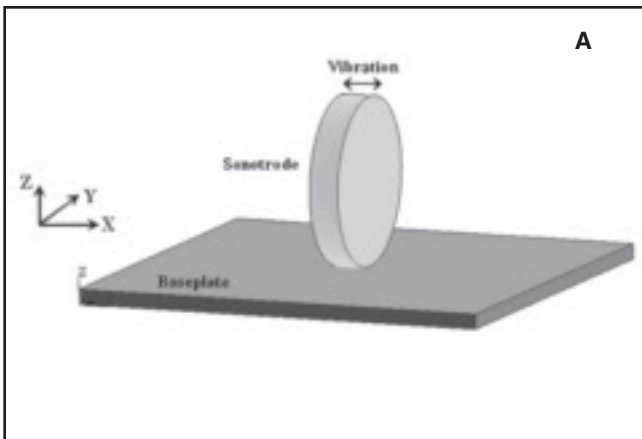


Fig. 3 — 3-D coupled-field model for ultrasonic consolidation

mechanical field the strain and stress are determined by the pressure load, friction force, and temperature-dependent material properties. In the thermal field, the temperature is assumed to be mainly influenced by the heat generated by friction. The friction coefficient and material mechanical properties vary with temperature, which in turn affect the heat generation.

material properties and quantities at the last time step must be determined for calculating the state at the current time step.

Finite Element Analysis

For the purpose of understanding the role of friction in UC and its contribution to the bond formation, a 3-D coupled-field

Two routes are believed to couple the mechanical and thermal fields in ultrasonic consolidation: 1) The thermal field affects the mechanical field, because most of the material mechanical properties, such as modulus of elasticity, yield strength, and friction coefficient, are temperature sensitive; and 2) the mechanical field (the friction force) generates heat, which changes the thermal field. During simulation, these varying

nonlinear model has been developed and a dynamic finite element analysis has been conducted based on the ANSYS package.

Theoretical Background

In the ANSYS mechanical analysis, the stress and strain relationship is as follows:

$$\{\sigma\} = [D]\{\epsilon^{el}\} \quad (1)$$

$$\{\epsilon^{el}\} = \{\epsilon\} - \{\epsilon^{pl}\} - \{\epsilon^{th}\} \quad (2)$$

where $\{\sigma\}$ is stress vector, $[D]$ is elastic stiffness matrix, which is a function of temperature, $\{\epsilon^{el}\}$ is elastic strain vector, $\{\epsilon\}$ is total strain vector, $\{\epsilon^{pl}\}$ is plastic strain vector, and $\{\epsilon^{th}\}$ is thermal strain vector.

The bilinear von Mises yield criteria are used in this model. If the von Mises equivalent stress is less than the material yield strength at temperature, the stress state is elastic and no plastic strain is computed. If the stress exceeds the material yield strength, the plastic strain ϵ^{pl} is calculated by

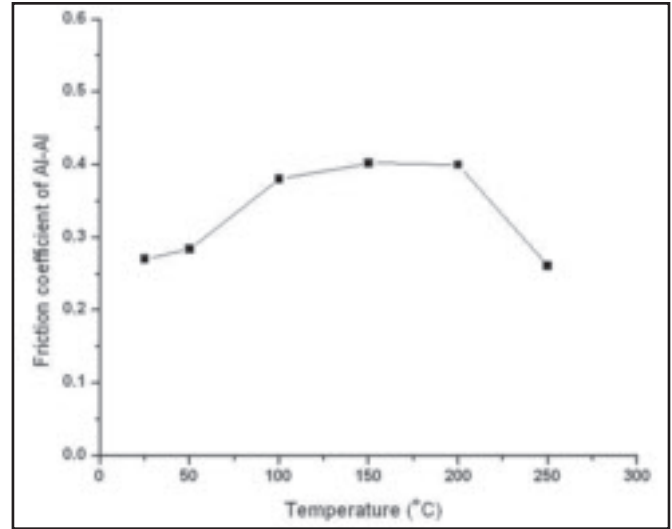
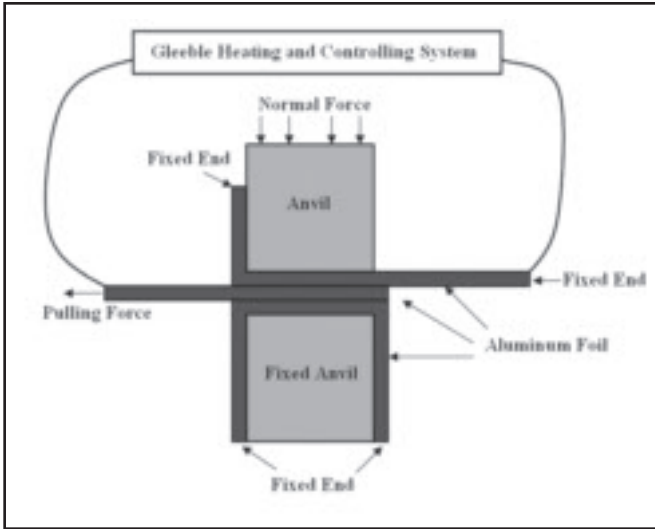


Fig. 4 — Schematic of Al-Al friction coefficient measurement on a Gleeble 1500D.

Fig. 5 — Al-Al friction coefficient varying with temperature (Ref. 13).

Table 1 — Element Types and Functions

Name	Description	Function
Solid92	3-D 10-node tetrahedral structural solid element	A
Solid227	3-D 10-node coupled-field solid element	B
Conta174 & Targe170	surface-to-surface contact element pair	both A and B

A — mechanical analysis; B — thermomechanical analysis

Table 2 — Temperature-Dependent Mechanical Properties of AL 3003-H18

Temp. (°C)	Modulus of Elasticity (GPa)	Yield Strength (MPa)	Yield Strength (Ref. 15) (MPa)
25	53.2	227.3	185
50	28.8	197.3	—
100	26.8	131.2	145
150	22.7	70.0	—
200	16.9	68.3	62
250	16.4	32.9	—
300	14.5	29.0	17
350	13.3	26.5	—

Table 3 — Nominal Chemical Composition of AL 3003-H18 (wt-%) (Ref. 15)

Al	Cu	Fe	Mn	Si	Zn
96.7–99.0	0.050–0.200	≤ 0.700	1.00–1.50	≤ 0.600	≤ 0.100

Table 4 — Thermal Properties of AL 3003-H18 (Ref. 15)

CTE (μm/m-°C)	Specific Heat (J/g-°C)	Thermal Conductivity (W/m-K)
25.1	0.893	155

$$\{\delta \epsilon^{pl}\} = \lambda \left\{ \frac{\partial Q}{\partial \sigma} \right\} \quad (3)$$

where λ is the plastic multiplier (which determines the amount of plastic straining) and Q is the yield function. As the material yields, the yield surface changes due to the bilinear isotropic (work) hardening.

To find out the effect of sonotrode's cyclic motion, a transient dynamic analysis is conducted on the model. The governing dynamic equation is as follows for a linear structure (Ref. 14):

$$[M] \left\{ \frac{\partial^2 u}{\partial t^2} \right\} + [C] \left\{ \frac{\partial u}{\partial t} \right\} + [K] \{u\} = \{F^a\} \quad (4)$$

where $[M]$ is the structural mass matrix, $[C]$ is the structural damping matrix, $[K]$ is the structural stiffness matrix, $\{\partial^2 u / \partial t^2\}$ is the nodal acceleration vector, $\{\partial u / \partial t\}$ is the nodal velocity vector, $\{u\}$ is the nodal displacement vector, and $\{F^a\}$ is the applied load vector. The nonlinear analysis in this model is preceded by updating these matrixes computed from the temperature-dependent material properties and conducting a linear analysis for each step.

In the ANSYS thermal module, conduction heat flow is included in the FEM model and the governing equation is as follows:

$$\rho c \left(\frac{\partial T}{\partial t} + (\vec{v} \cdot \nabla) T \right) = \dot{q} + \nabla \cdot ((\vec{K} \cdot \nabla) T) \quad (5)$$

where ρ is density, c is specific heat, T is temperature, t is time, \vec{v} is velocity vector for mass transport of heat, \dot{q} is heat gen-

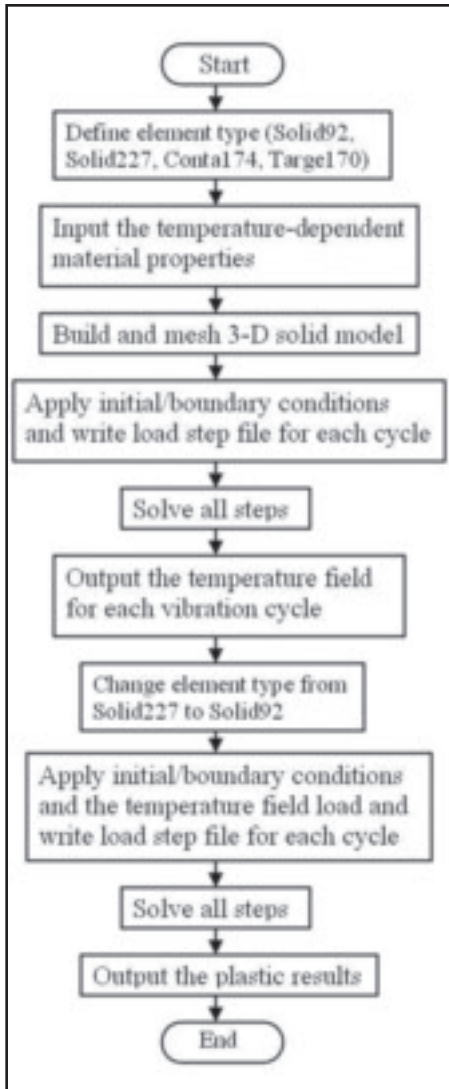


Fig. 6 — Flowchart of finite element analysis for UC.

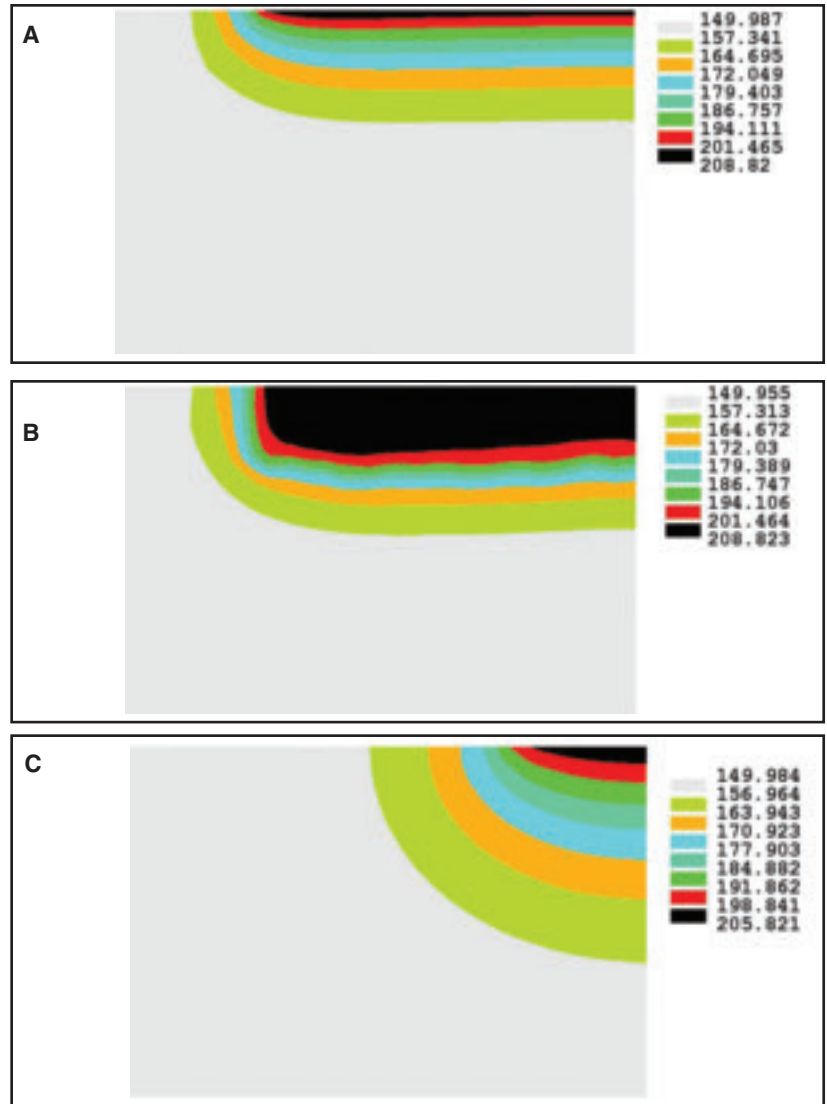


Fig. 7 — Distribution of temperature (°C) at the 1500th vibration cycle. A — Front view; B — top view; and C — side view.

eration rate per unit volume, \dot{K} is conductivity vector, and $\nabla = \partial/\partial x + \partial/\partial y + \partial/\partial z$.

In the ANSYS thermomechanical coupled analysis, the thermal-structural coupled finite element matrix equation derived from the stress equation of motion and the heat flow conservation equation coupled by the thermoelastic constitutive equations is as follows (Ref. 14):

$$\begin{bmatrix} [M] & [0] \\ [0] & [0] \end{bmatrix} \begin{Bmatrix} \{\dot{u}\} \\ \{\dot{T}\} \end{Bmatrix} + \begin{bmatrix} [C] & [0] \\ [C^{tu}] & [C^t] \end{bmatrix} \begin{Bmatrix} \{\dot{u}\} \\ \{\dot{T}\} \end{Bmatrix} + \begin{bmatrix} [K] & [K^{tu}] \\ [0] & [K^t] \end{bmatrix} \begin{Bmatrix} \{u\} \\ \{T\} \end{Bmatrix} = \begin{Bmatrix} \{F\} \\ \{Q\} \end{Bmatrix} \quad (6)$$

where $[M]$ is the element mass matrix, $[C]$ is the element structural damping matrix, $[K]$ is the element stiffness matrix, $\{u\}$ is the displacement vector, $\{F\}$ is the sum of

the element nodal force, $[C^t]$ is the element specific heat matrix, $[K^t]$ is the element diffusion conductivity matrix, $\{T\}$ is the temperature vector, $\{Q\}$ is the sum of the element heat generation load and element convection surface heat flow vectors, $[K^{tu}]$ is the element thermoelastic stiffness matrix ($= -\int_{vol} [B]^T \{\beta\} \{\nabla \{N\}^T d\{vol\}$), $[B]$ is the strain-displacement matrix, $[C^{tu}]$ is the element thermoelastic damping matrix ($= -T_o [K^{tu}]^T$), T_o is the absolute reference temperature ($= T_{ref} + T_{off}$), T_{ref} is the reference temperature.

Finite Element Model

Figure 3A shows the 3-D UC model with the sonotrode located at the center of the baseplate. The dimensions of the baseplate and cylindrical sonotrode are the

same as the experimental setup: $355.6 \times 355.6 \times 12.7$ mm and 146.1 mm (diameter) $\times 25.4$ mm (thickness). Compared with the baseplate and sonotrode, the aluminum foil is much smaller (25.4 mm width and 0.1 mm thickness). Since this model has two symmetrical planes (Plane X = 177.8 mm and Plane Y = 177.8 mm) and the large difference in dimensions exists between the foil and baseplate/sonotrode, a UC model with quarter size has been built and shown in Fig. 3B. This model is used to simulate the bonding of the first layer. Because the foil is very thin and the sonotrode has a roughened surface, it is assumed that a no-slip condition exists between the top surface of the foil and the sonotrode. The friction is assumed to occur between the bottom surface of the foil and the substrate. The 3-D coupled-field meshed model (Fig.

3C) involving the sonotrode that is in close contact with and vibrates against the substrate has been developed. The meshing around the contact area is refined following a meshing study. The type of elements used in simulation and their functions are listed in Table 1. The number of total nodes and elements is 14722 and 10251, respectively.

Material Properties

Tensile tests have been conducted on the Gleeble 1500D thermal-mechanical simulator for measuring the temperature-dependent mechanical properties of aluminum foil (Al 3003-H18) used in this study. The dimensions of test samples are $22.0 \times 10.1 \times 0.1$ mm, and the tensile load rate is 1.2 mm/min. Specimens were heated to various temperatures and held for 3 min for thermal equilibrium, and tensile pulled. The results are listed in Table 2. It is seen that the properties of aluminum material are very sensitive to the temperature. At the preheating temperature (150°C), the mechanical properties decrease to the half or even less of those at room temperature. The measured yield strength data of aluminum foil are different, but close to those from the reference. The composition and thermal properties for Al 3003-H18 are shown in Tables 3 and 4.

Coulomb's law of friction is used to simulate the friction-like shear force on the bonding interface. Since the pressure is constant in the process, the friction coefficient is the only factor determining the magnitude of friction. Experiments for measuring the Al-Al friction coefficient have been designed and conducted on the Gleeble 1500D. Figure 4 shows the device setup. The fixed anvil is covered with foil of Al 3003-H18 and another foil is put between them. A normal force (N) is applied on the top anvil. When a certain uniform temperature is achieved by the heating and controlling system of the Gleeble, the middle foil is pulled out at a certain rate (sliding speed). The sliding speeds between 1 and 1000 mm/s are tested. The friction occurs on the top and bottom surfaces of the foil pulled out. Therefore, the Al-Al friction coefficient at the testing temperature can be calculated by $\mu = F/2(N + W)$, where F is the measured pulling force, and W is the top anvil's weight and pressure. Friction coefficient of Al-Al varying with temperature is shown in Fig. 5. There is no significant effect of sliding speeds, in the range tested, on the friction coefficient.

The model in this paper has included the material nonlinear effects by using the data in temperature-dependent mechanical properties tables above. In the transient dynamic analysis, the mechanical properties for different locations on the contact surface are different depending

on the local temperature and are input to the model for each step.

Boundary and Initial Conditions

The UC process parameters, including pressure load (1800 N), preheating temperature (150°C), vibration amplitude (16 μ m), and vibration frequency (20 kHz), are incorporated in the model as boundary conditions. The pressure load and vibrational displacement are applied to the interface of foil and baseplate. A triangle wave is used to approximate the sinusoidal waveform of the ultrasonic vibration. The measured contact area under 1800 N is 4.7 mm along the direction of the sonotrode's moving, and the sonotrode's speed in UC process is 28 mm/s. For a given point underneath the sonotrode, the maximum time of contact is approximately 0.16 s, or about 3000 cycles of vibration. Therefore, we assume a stationary sonotrode in the model, and the maximum number of cycles to be modeled is 3000.

A fixed boundary condition for displacement is applied to the baseplate's bottom surface and all corners except the surface contacting the sonotrode. Symmetrical boundary conditions are used on two symmetrical planes. A uniform initial preheating temperature is applied to the parts around the bonding surface, including the sonotrode, baseplate, and foil. No convective heat loss from baseplate and sonotrode to air is assumed because the UC device is in an enclosed space in which there is no significant air flow. The radiation heat loss is also ignored due to the low temperature range.

Methodology of Finite Element Analysis for UC

Because of the limit of capability of the ANSYS thermomechanical coupled element, no plastic results can be obtained from the thermoelastic equation. Therefore, the strategy for simulation involves calling appropriate analysis modules: 1) Conduct a thermoelastic analysis using the thermomechanical coupled element for friction heat generation; 2) output the temperature data for each node; 3) change the element type to the mechanical element; 4) apply the temperature load

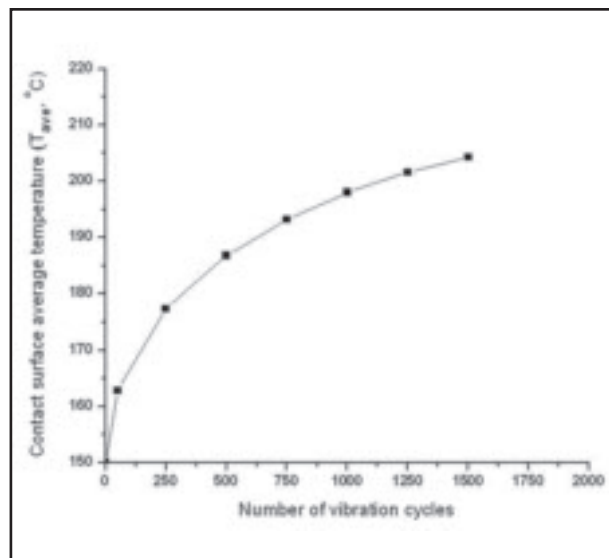


Fig. 8 — Average temperature at the contact surface as a function of the vibration cycle.

on each node; and 5) conduct a mechanical analysis and output the plastic results. A flowchart that outlines the analysis procedures is given in Fig. 6. A further simplification involves that the plastic deformation is assumed to have no effect on the friction heat generation, and that no plastic heat is generated in the entire process.

Simulation Results

Effect of Friction on Temperature

Figure 7 shows the coordinate plane projections of temperature distribution on the contact surface (bond interface) at the 1500th vibration cycle. With friction heat, a uniform peak temperature state exists on the contact surface, and the temperature decreases away from the contact surface into the substrate. The temperature distribution shows a cylindrical symmetry about the center of the contact surface.

The average temperature due to friction at the contact surface increases rapidly with the number of vibration cycles in the initial period of bonding. As the welding time is longer (higher number of cycles), the temperature rise slows down, and seems to approach a steady state — Fig. 8. The increase of interface temperature is influenced by $q_{friction} - q_{loss}$, where $q_{friction}$ is the friction heat generation rate, $q_{loss} = \kappa \Delta T$ is the heat dissipation rate by conduction. At the beginning of UC bonding, the rate of friction heat generation is much higher than that of heat loss, because initially the temperature difference (ΔT) is low. As the temperature becomes higher due to friction heating, two com-

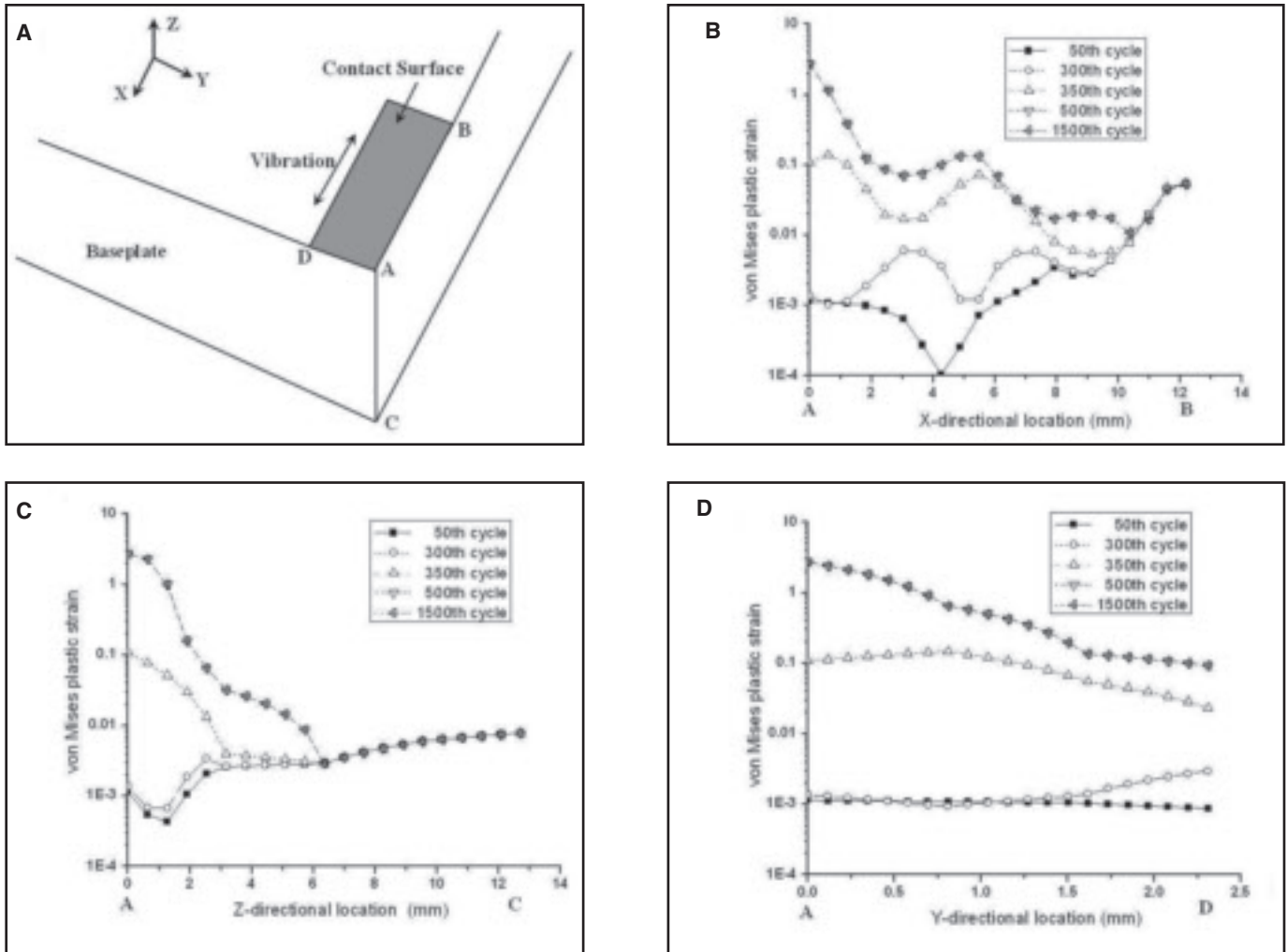


Fig. 9 — Distribution of plastic strain as a function of location and vibration cycle.

peting factors become significant: On the one hand, the decrease of Young's modulus (Table 2) and friction coefficient (Fig. 5) will slow down the friction heat generation; on the other hand, the greater temperature difference enhances faster heat dissipation. Therefore, the temperature increase slows down. A balance between $q_{friction}$ and q_{loss} can be achieved eventually, giving rise to $q_{friction} - q_{loss} = 0$, i.e., a thermal steady state. Physically, if the heat loss is faster than the friction heat generation and the interface temperature decreases, the higher values of Young's modulus and friction coefficient at the lower temperature will automatically increase the $q_{friction}$ until a new dynamic heat balance is achieved.

Effect of Friction on Plastic Deformation

Three paths (A-B, A-C, and A-D) have been selected to show the three-dimensional distributions of von Mises strain

around the contact surface where the bonding process happens — Fig. 9A. Figure 9B shows the von Mises strain distributions along path A-B (the vibration direction) as a function of the number of vibration cycles. At the beginning of bonding (50th cycle), the plastic strain is relatively small. The highest plastic strain occurs at the edge of the contact surface near point B. By the 350th cycle, the plastic strain in the center of the contact surface exceeds the level of plastic strain at the edge. After the 500th vibration cycle, the value and distribution of plastic deformation reach a steady state, when there is no change in von Mises strain with further increase of the vibration cycle. The maximum plastic strain is located at point A, the center of the contact surface. A wavy-shaped plastic strain distribution caused by the cyclic vibration is apparent. The reason for such characteristic wave shape distribution of deformation has been studied and explained by superposition of vi-

bration waves in Ref. 9.

A similar plastic strain distribution can be seen along path A-C (the depth direction). In Fig. 9C, a small region close to point A has a plastic strain level higher than 1 after 500 vibration cycles. The depth direction plastic strain in all other regions along path A-C is lower than 0.1. Since the depth direction plastic strain is the easiest to measure experimentally, it will be used for verification of the model later.

Path A-D is perpendicular to the sonotrode vibration; therefore, there is no waveshape deformation distribution (Fig. 9D) as seen along path A-B. A steady increase of plastic strain levels can be seen as the number of cycles increases. The steady-state strain distribution indicates a peak level close to point A.

The evolution of the average von Mises plastic strain on the contact surface as a function of time (or vibration cycle) is shown in Fig. 10. It has the same trend as the temperature vs. vibration cycle in Fig.

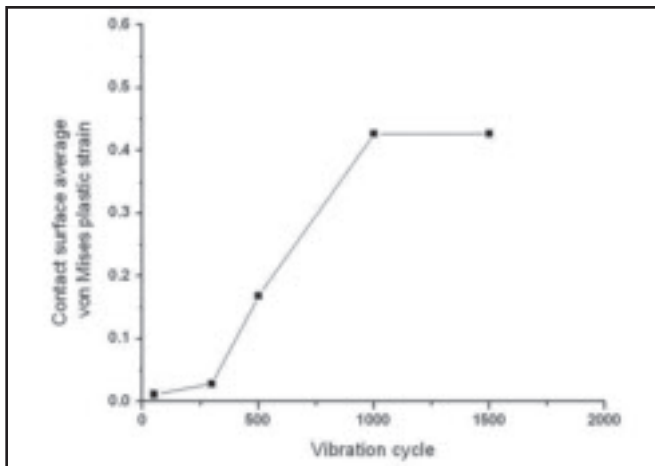


Fig. 10 — Average plastic strain at the contact surface as a function of vibration cycle.

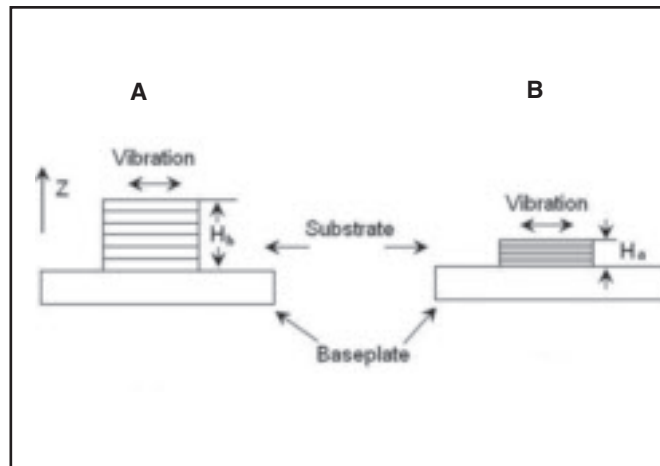


Fig. 11 — Schematic of preferment deformation in substrate's height (Ref. 13).

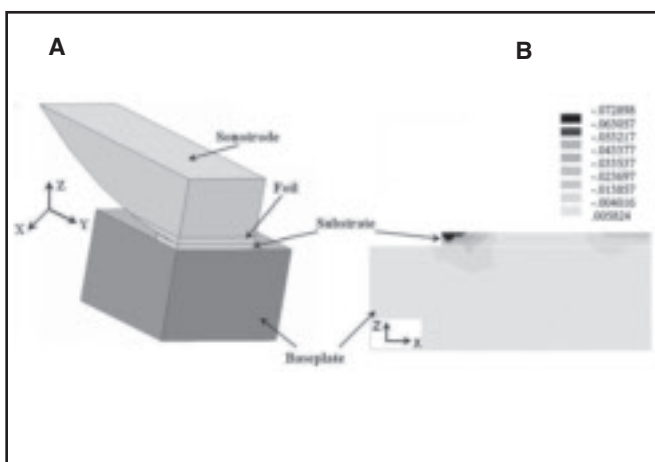


Fig. 12 — A — 3-D coupled-field model for validation; B — distribution of z-directional plastic strain for an eight-layer deposit.

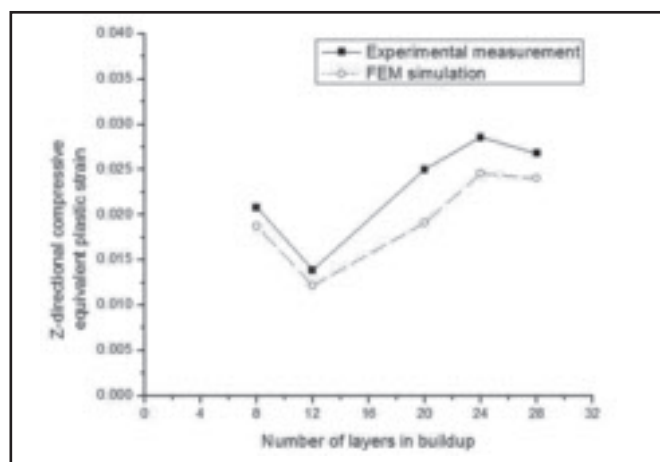


Fig. 13 — Comparison of experimental measurements and simulation results for the average z-direction compressive plastic strain (Ref. 13).

8. The average plastic strain also approaches a “steady state” at the 1000th vibration cycle when the contact surface average temperature is close to the steady state. The time to reach the steady state for the average plastic strain is later than that for the three paths defined in Fig. 9.

In the initial period when the temperature is increasing, the yield strength of material in the contact area decreases. When the von Mises stress at any location reaches the yield condition at certain specific temperature, the material yields and plastic deformation occurs. When the friction heat generation on the interface balances the heat loss and the average temperature approaches the steady state, the increase in plastic deformation stops and a similar steady state is also achieved. The number of cycles to reach this steady state may decrease (or the time may be shorter) when plastic deformation heat is consid-

ered in addition to the friction heat.

One important experimental observation in UC is that the strongest bonding is only achieved with an optimized travel velocity of the sonotrode. Too fast travel velocity does not provide enough dwell time (or number of vibration cycles) for bonding; while too slow a travel velocity does not result in good bonding either. The evolution of temperature and plastic strain obtained in this study can help quantitatively understand the phenomena, and provide control strategies for stronger bonding.

FEM Model Validation

Definition of Z-Directional Compressive Equivalent Plastic Strain in Experiment

An experimental validation of the finite element results shown in Fig. 9C was

conducted. In UC, the height of deposit is smaller than the sum of foil layers' original thickness, and the relative ratio is changing with the number of layers. Figure 11 shows the difference of substrate's height before bonding (A) and after bonding (B). Thus, the z-directional compressive equivalent plastic strain can be defined as follows:

$$\epsilon_{z,eq}^{pl} = \frac{(H_a - H_b)}{H_b} \quad (7)$$

Samples of various numbers of layers are made on the UC machine with the same process parameters used in the simulations. The sample heights after UC bonding are measured with a precision height gauge with a 0.001-mm resolution. The substrate's height before bonding is calculated by 0.1 mm (foil thickness) × 8 (layer's number). Thus, the z-directional compressive

equivalent plastic strain from the experiment can be calculated by Equation 7.

Definition of Z-Directional Compressive Equivalent Plastic Strain in Simulation

For the purpose of finite element model validation, a new finite element model is developed to incorporate a rectangular substrate 12.2 mm long and 5.0 mm wide — Fig. 12A. The same simulation strategy is applied to the new simulation with various buildup layers. A cut section plane parallel to the vibration direction and located at the center of the substrate is chosen for extracting the z-directional plastic strain. Figure 12B shows the distribution of z-directional plastic strain in the cut section for the eight layers of the substrate. The average value is calculated and defined as the z-directional compressive equivalent plastic strain in simulation.

Comparison

Figure 13 shows the comparison of z-directional compressive equivalent plastic strain between experiment measurement and finite element simulation. It can be seen that the finite element model in this paper is able to correctly predict the trend and magnitude of the experimental data. The error may be very likely due to the omission of contribution of plastic heat flux to plastic strain. Another error source is the use of solid substrate in the validation model instead of the true substrate that actually has a layered structure and different mechanical properties. When the temperature increases, the tendency for microstructure change, such as recovery, which is not included in the model,

may also contribute to the error.

Conclusions

1. A friction-based dynamic, coupled-field, finite element model has been developed for ultrasonic consolidation. The friction heat flux at the bond interface increases quickly in the initial period of bonding and approaches a steady state. The peak temperature develops at the bond interface due to friction heating.

2. The plastic strain is believed to contribute to bond formation of the ultrasonic consolidation. Similar to the temperature field, the plastic strain field also approaches a steady state after a certain number of vibration cycles. The peak level of the plastic strain is located near the center of the contact surface between the top foil and substrate. The plastic strain has a characteristic waveshape distribution that is caused by the superposition of vibration waves.

3. The model has been reasonably verified by experimental measurement. The results are able to provide insights for understanding the mechanisms of bond formation for ultrasonic consolidation, and for guiding experimental design for stronger ultrasonic bonds.

Acknowledgment

This work was supported by the National Science Foundation through DMI-0522908.

References

1. *Welding Handbook* 1991. Welding process. Vol. 2, pp. 783–812. R. L. O'Brien, ed. Miami, Fla.: American Welding Society.

2. Daniels, P. C. 1965. Ultrasonics. *Ultrasonic welding* 3(4): 190–196.

3. Rawal, S. 2001. Metal-matrix composites for space applications. *JOM* 53(4): 14–17.

4. Jones, J., and Meyer, F. 1958. Ultrasonic welding of structural aluminum alloys. *Welding Journal* 37(3): 81-s to 92-s.

5. Joshi, K. 1971. The formation of ultrasonic bonds. *Welding Journal* 50(12): 840–848.

6. Kong, C. Y., Soar, R. C., and Dickens, P. M. 2005. Ultrasonic consolidation technique for embedding sma fibers with aluminum matrices. *Composite Structures* 66: 421–427.

7. Doumanidis, C., and Gao, Y. 2002. Mechanical modeling of ultrasonic welding. *Welding Journal* 83(4): 140-s to 146-s.

8. de Vries, D. 2004. Mechanics and mechanisms of ultrasonic metal welding. PhD thesis, The Ohio State University, Columbus Ohio.

9. Zhang, C., and Li, L. 2006. A study of dynamic mechanical behavior of substrate in ultrasonic consolidation. *The 17th Solid Freeform Fabrication Symposium, Austin, Tex.*

10. Kong, C. Y., Soar, R. C., and Dickens, P. M. 2005. A model for welding strength in ultrasonically consolidated components. *Proceedings of the Institution of Mechanical Engineers, Part C: Journal of Mechanical Engineering Science* 219(1): 83–91.

11. Gao, Y., and Doumanidis, C. 2002. Mechanical analysis of ultrasonic bonding for rapid prototyping. *Journal of Manufacturing Science and Engineering, Transactions of the ASME* 124(2): 426–434.

12. White, D. R. 2003. Ultrasonic consolidation of aluminum tooling. *Advanced Materials & Processes* 161(1): 64, 65.

13. Zhang, C., and Li, L. 2007. Effect of friction on ultrasonic consolidation. *Proceedings of the 2007 International Manufacturing Science and Engineering Conference, ASME* (paper number MSEC2007-31202).

14. ANSYS, Inc. *Release 11.0 Documentation for ANSYS*.

15. *Metals Handbook*, Vol. 2. Oct. 1990. ASM International, 10th edition.

Call for Papers

15th International Conference on the Joining of Materials

The 15th International Conference on the Joining of Materials (JOM-15) and the 6th International Conference on Education in Welding (ICEW-6) Conference and Exhibition organized by the JOM Institute and supported by Dansk Metal, Danish Welding Society, and DSL FORCE Technology, will be held May 3–6, 2009, Helsingør, Denmark.

A full technical program on welding technology and education and training will be conducted. The main topics are listed below.

- 1) Recent developments in joining technology — welding, soldering, brazing, and projects, with the emphasis on industrial applications,
- 2) Welding quality — properties and environmental considerations,
- 3) Welding management and qualification of welding personnel.

The organizers cordially invite you to send a title of your presentation and a short abstract by October 15, 2008. Notification of acceptance and author's guidelines will follow after review of the abstracts by December 2008. Full papers must be received by February 2009. Please send your name, address, title, and abstract to Alan Parnes (Dansk Metal); e-mail alan.parnes@danskmetal.dk. For further information about the conference, contact JOM, Gilleleje Strandvej, 28 DK-3250 Gilleleje, Denmark. Telephone: +45 48355458, e-mail jom_aws@post10.tele.dk.